2021 The 21st International Conference on Control, Automation and Systems (ICCAS 2021)
Ramada Plaza Hotel, Jeju, Korea, Oct. 12∼15, 2021

Dynamic Obstacle Avoidance of Multi-rotor UAV using Chance Constrained MPC

Takumi Wakabayashi[1], Yuma Nunoya[1] and Satoshi Suzuki[1*]

[1]Department of Mechanical Engineering, Chiba University
Chiba, Japan (suzuki-s@chiba-u.jp) * Corresponding author

Abstract: Recently, in order to carry out tasks efficiently such as infrastructure inspection and goods transportation, operations using multi-rotor Unmanned Aerial Vehicles (UAVs) in formation flight are often considered. One of the main issues in motion planning among multiple UAVs is collision avoidance. Model Predictive Control (MPC) is characterized by its ability to consider collision avoidance in the framework of constrained optimization. For this reason, there have been many studies on collision avoidance using MPC, but few studies take into account the uncertainty that occurs in real environments. On the other hand, Chance constrained MPC (CCMPC) is considered to be more robust in collision avoidance due to the consideration of uncertainty. However, the structure of the collision probability constraint equation to be introduced into the evaluation function of MPC has not been sufficiently studied. In this study, the structure of equations for incorporating probability constraints into the evaluation function is examined. Moreover, by quantitatively comparing the equations with the same structure with deterministic constraints introduced into the evaluation function, the difference in collision avoidance is clarified.

Keywords: Collision avoidance, path planning for multiple UAVs, formation flight.

1. INTRODUCTION

In recent years, multi-rotor unmanned aerial vehicles (UAVs) are expected to be used in industrial applications such as infrastructure inspection and goods transportation for the purpose of unmanned and manpower-saving operations. In particular, small UAVs weighting less than 5 kg are attracting attention for their ease of handling [1]. However, They have strict limitations in terms of payload and endurance. In order to solve these problems, research on formation flight using multiple small UAVs has been conducted [2][3]. The demand for industrial applications of small multi-rotor UAVs in formation flight is considered to growing. The main advantages of formation flight are improved work efficiency and fault tolerance. For example, by loading different sensors and manipulators on multiple UAVs to perform different tasks, the overall work efficiency can be improved.

One of the technical issues in operating UAVs in formation flight is collision avoidance with multiple UAVs and obstacles. There are several collision avoidance methods such as artificial potential field and reciprocal velocity obstacles[4][5]. However, those methods have the local minima issue where UAVs can be trapped. For example, in artificial potential field algorithm, it is necessary to form an appropriate potential field that will result in the target behavior in order to converge to the target value, and to obtain the control input. On the other hand, when Model Predictive Control (MPC) is used, deadlocks are considered to be less likely to occur, because collision avoidance can be taken into account within the framework of constrained optimization. For this reason, many studies on collision avoidance have been conducted using MPC, such as [2][3][6]. Although there is a method to avoid collisions between UAVs in formation flight by communicating with each other [7], the computational cost increases with the increase in the number of UAVs, and there are issues with the stability of communication. For collision avoidance against static obstacles, there are methods called roadmap and rapidly-exploring random trees [8][9]. These methods have the advantage of efficiently generating avoidance trajectories by globally navigating. In contrast to static environments, where the position and velocity of obstacles vary with time and uncertainty, it may not be possible to generate optimal avoidance trajectories in real time. In particular, in outdoor environments, there is a possibility that collisions between UAVs and birds called bird strike, can be a problem. Collision avoidance with birds involves more uncertainty than avoidance between UAVs. In addition, errors such as sensor errors and maneuver errors, occur in the real environment.

Chance constrained MPC (CCMPC) is a collision avoidance method that can take into account the collision probability[10]. This method was shown to be robust to avoidance even in uncertain environments by considering collision probability as a constraint. However, the structure of the collision probability constraint equation to be introduced into the evaluation function of MPC has not been examined. Although [11] and [12] are given as comparison methods in the previous study, they differ not only in the constraint equations but also in the structure of the equations used to introduce them into the evaluation function. Consequently, the evaluation of the difference in collision avoidance due to the use of collision probability constraints is considered insufficient. In this study, the structure of equations for incorporating probability constraints into the evaluation function is examined. Moreover, by quantitatively comparing the equations with the same structure with deterministic constraints introduced into the evaluation function, the difference in collision

2021 21st International Conference on Control, Automation and Systems (ICCAS) | 978-89-93215-21-2/21/$31.00 ©2021 10.23919/ICCAS52745.2021.9649942

avoidance is clarified. The rest of this paper is organized as follows. UAV and obstacle model are presented in Section 2. In Section 3, the collision avoidance method using CCMPC is described. We present simulation results in Section 4. Finally, conclusion of this work is shown in Section 5.

2. MODELING

In this section, the UAV model and obstacle model are described. In this paper, vectors are denoted in bold letters $\boldsymbol{x}$, matrices in capital A, and sets in mathcal $\mathcal{A}$. A hat $\hat{x}$ denotes the mean of random variables x, $Pr(\cdot)$ indicates the probability of an event and a superscript denotes transpose of $\boldsymbol{x}^T$.

2.1 UAV model

In this paper, the number of UAV is n, and each UAV is denoted by a subscript $i \in \mathcal{I} = \{1, 2 \dots n\}$. The dynamics of each UAV $i \in \mathcal{I}$ are described by a discrete-time model,

$$\boldsymbol{x}_i^{k+1} = \boldsymbol{f}_i(\boldsymbol{x}_i^k, \boldsymbol{u}_i^k) + \boldsymbol{\omega}_i^k, \quad \boldsymbol{x}^0 \sim \mathcal{N}(\hat{\boldsymbol{x}}_i^0, \Gamma_i^0) \quad (1)$$

where $\boldsymbol{x}_i^k = [\boldsymbol{a}_i^k, \boldsymbol{v}_i^k, \boldsymbol{p}_i^k, {}^s\boldsymbol{v}_i^k]^T$ is the state of the UAV, which denotes acceleration, velocity, position, and sensor velocity at time k. The sensor velocity is the velocity that considers the delay time in the x-axis and y-axis acquired by the sensor. $\boldsymbol{u}_i^k = [\phi_i^k, \theta_i^k, \psi_i^k, {}^zV_i^k]^T$ is the control inputs which represents the attitude command value of the three axes and the velocity command value of the z-axis. The initial state $\boldsymbol{x}_i^0$ is random variable considered as a Gaussian distribution with mean $\hat{\boldsymbol{x}}_i^0$ and covariance matrix Γ_i^0. These are given by a state estimator such as a Kalman Filter. $\boldsymbol{f}_i$ denotes the dynamics of the UAV, with attitude and angular velocity under control. $\boldsymbol{\omega}_i^k$ denotes process noise, which is $\boldsymbol{\omega}_i^k \sim \mathcal{N}(0, Q_i^k)$. In this study, we adopt Liberaware's IBIS as a control target. The overview of the IBIS is shown in Fig.1. For the simplicity, shape of the UAV is assumed to be a sphere of radius r_i.

2.2 Obstacle model

Each obstacle is denoted as $o \in \mathcal{I}_o = \{1, 2, ..., n_o\}$ and its position as $\boldsymbol{p}_o = [x, y, z]^T$. An obstacle is modeled as an ellipsoid with each axis represented by (a_o, b_o, c_o) as shown Fig. 2 (a). In the prediction interval of CCMPC, it is assumed that the obstacle is in constant velocity linear motion. The position of the obstacle is predicted by assuming that it contains Gaussian noise with a mean value of zero.

3. CHANCE CONSTRAINED MPC

MPC obtains the control input by solving an optimization problem in real time to minimize the evaluation function in the prediction interval. CCMPC is characterized by the use of a constraint in the evaluation function to keep the collision probability below a threshold. In this section, the collision is defined and then chance constraints is described. After that, evaluation functions and constraints used in this study are described.

Fig. 1.: Overview of the IBIS

3.1 Collision detection

The collision between UAV i and UAV j at time k is defined as follows.

$$C_{ij}^k := \{\boldsymbol{x}_i^k | \|\boldsymbol{p}_i^k - \boldsymbol{p}_j^k\| \leq r_i + r_j\} \quad (2)$$

Since determining the collision with an ellipsoid obstacle is complex, the ellipsoid is enlarged by the radius r_i of the UAV as shown in Fig.2 (b), and an affine transformation is performed as shown in Fig.2 (c). A collision is determined based on whether the coordinates of the center of the sphere, which is the position of the center of gravity of the UAV, is within this area.

$$C_{io}^k := \{\boldsymbol{x}_i^k | \|\boldsymbol{p}_i^k - \boldsymbol{p}_o^k\|^T \Omega_{io} \|\boldsymbol{p}_i^k - \boldsymbol{p}_o^k\| \leq 1\} \quad (3)$$

where $\Omega_{io} = R_o^T diag(1/(a_o + r_i)^2, 1/(b_o + r_i)^2, 1/(c_o + r_i)^2) R_o$, and R_o denotes the rotation matrix of the obstacle.

3.2 Chance constraints

In this paper, the position of the UAV and an obstacle is determined by a randomly chosen probability distribution, and the collision avoidance constraint is described as follows.

$$Pr(\boldsymbol{x}_i^k \notin C_{ij}^k) \geq 1 - \delta_r, \qquad \forall j \in \mathcal{I}, j \neq i \quad (4)$$

$$Pr(\boldsymbol{x}_i^k \notin C_{io}^k) \geq 1 - \delta_o, \qquad \forall o \in \mathcal{I}_o \quad (5)$$

Let δ_r, δ_o denotes thresholds that represent the collision probability.

3.3 Evaluation function

MPC solves an optimization problem to be minimized within a finite time period set by an evaluation function. The evaluation function is described as follows.

$$J = \varphi(\bar{\boldsymbol{x}}(t+T)) + \int_t^{t+T} (L(\bar{\boldsymbol{x}}(t+\tau), \bar{\boldsymbol{u}}(t+\tau)) d\tau \quad (6)$$

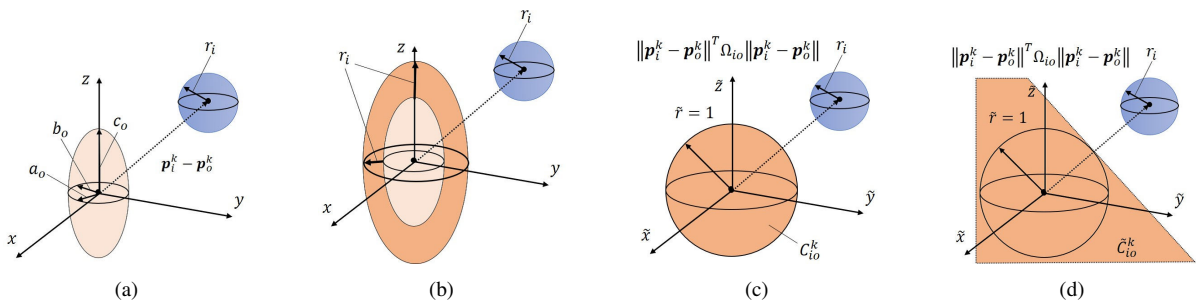

Fig. 2.: Collision detection between the UAV and an obstacle. (a) Position of the UAV and an obstacle. (b) Expanding each axis of the ellipsoid by the radius of the UAV. (c) Affine transformation to a sphere of radius 1. (d) Half space perpendicular to the relative position vector between the UAV and an obstacle.

T and τ denote the time that represents the evaluation interval and the time variable within the evaluation interval from the current time t. In addition, $\bar{\boldsymbol{x}}$ and $\bar{\boldsymbol{u}}$ denote the state and control inputs estimated by the model in the prediction interval. The first and second terms are called terminal cost and stage cost, and are described as follows.

$$\varphi\ (\bar{\boldsymbol{x}}(t+T)) = \bar{\boldsymbol{x}}^T(t+T)S\bar{\boldsymbol{x}}(t+T) \tag{7}$$

$$L\ (\bar{\boldsymbol{x}}(t+\tau), \bar{\boldsymbol{u}}(t+\tau)) = \bar{\boldsymbol{x}}^T(t+\tau)Q\bar{\boldsymbol{x}}(t+\tau) \tag{8}$$
$$+\ \bar{\boldsymbol{u}}^T(t+\tau)R\bar{\boldsymbol{u}}(t+\tau)+l_1P(\bar{\boldsymbol{x}}(t+\tau))+l_2B(\bar{\boldsymbol{x}}(t+\tau))$$

Here, $P(\cdot)$ and $B(\cdot)$ denote the penalty function and barrier function. $S\,, Q\,, R$ are weighting matrices, and l_1, l_2 are the coefficients of the penalty and barrier functions.

3.4 Chance constraints with barrier functions

The constraint by collision probability proposed in the previous study is evaluated using a barrier function.[10]. The barrier function is a function that keeps the UAV under a defined constraint by rapidly increasing the cost when the UAV attempts to violate the acceptable region. In this section, we outline the collision probability constraints used in previous studies. Collision in prediction is defined by whether or not the UAV is in the half-space $\tilde{C}_{io}^k$ perpendicular to the relative vector of the UAV to the obstacle, as shown in Fig.2 (d). The collision probability constraint between UAVs is described,

$$g_{ij}^B(\boldsymbol{x}) = \boldsymbol{a}_{ij}^T(\hat{\boldsymbol{p}}_i - \hat{\boldsymbol{p}}_j) - b_{ij} \tag{9}$$
$$-\ \mathrm{erf}^{-1}(1-2\delta_r)\sqrt{2\boldsymbol{a}_{ij}^T(\Sigma_i+\Sigma_j)\boldsymbol{a}_{ij}}$$

where $\boldsymbol{a}_{ij} = (\hat{\boldsymbol{p}}_i - \hat{\boldsymbol{p}}_j)/\|\hat{\boldsymbol{p}}_i - \hat{\boldsymbol{p}}_j\|$, and $b_{ij} = r_i + r_j$. Σ_i and Σ_j are the error covariance matrices of UAV i and j. Similarly, the constraint equation on the collision probability between the UAV and an obstacle can be derived as follows.

$$g_{io}^B(\boldsymbol{x}) = \boldsymbol{a}_{io}^T(\tilde{\hat{\boldsymbol{p}}}_i - \tilde{\hat{\boldsymbol{p}}}_o) - \tilde{b}_{io} \tag{10}$$
$$-\ \mathrm{erf}^{-1}(1-2\delta_o)\sqrt{2\boldsymbol{a}_{io}^T(\tilde{\Sigma}_i+\tilde{\Sigma}_o)\boldsymbol{a}_{io}}$$

Here, $\tilde{\boldsymbol{y}} = \Omega_{io}^{\frac{1}{2}}\boldsymbol{y}$ denotes that an affine transformation has been performed, $\boldsymbol{a}_{io} = (\tilde{\hat{\boldsymbol{p}}}_i - \tilde{\hat{\boldsymbol{p}}}_o)/\|\tilde{\hat{\boldsymbol{p}}}_i - \tilde{\hat{\boldsymbol{p}}}_o\|$ and $\tilde{b_{io}} = 1$. The barrier function to be introduced in the evaluation function is represented as follows.

$$B(\boldsymbol{x}) = \frac{1}{g_{ij}^B(\boldsymbol{x})^2} + \frac{1}{g_{io}^B(\boldsymbol{x})^2} \tag{11}$$

3.5 Area constraint by penalty function

Constraints are placed around other UAV and obstacles in an area called the potential field to avoid entering the area. The constraint conditions are shown as follows.

$$g_{ij}^P(\boldsymbol{x}) = 1 - \|\hat{\boldsymbol{p}}_i - \hat{\boldsymbol{p}}_j\|^T\Omega_{ij}^{safe}\|\hat{\boldsymbol{p}}_i - \hat{\boldsymbol{p}}_j\| \tag{12}$$

Note that the plane does not tilt significantly, so it is represented as $\Omega_{ij}^{safe} = diag(1/(r_i + r_j + d_{ij}^a)^2, 1/(r_i + r_j + d_{ij}^b)^2, 1/(r_i + r_j + d_{ij}^c)^2)$. The safety region can be enlarged by d_{ij}^a, d_{ij}^b, d_{ij}^c in each axial direction. Fig.3 shows an example of applying the potential field to an obstacle. In this study, the potential field can be set more flexibly. The penalty function between UAVs to be introduced in the evaluation function is represented as follows.

$$P_{ij}(\boldsymbol{x}) = \begin{cases} g_{ij}^P(\boldsymbol{x}), & if\ g_{ij}^P(\boldsymbol{x}) \geq 0 \\ 0, & (otherwise) \end{cases} \tag{13}$$

Similarly, the constraint condition between the UAV i and the obstacle is shown as follows.

$$g_{io}^P(\boldsymbol{x}) = 1 - \|\hat{\boldsymbol{p}}_i - \hat{\boldsymbol{p}}_o\|^T\Omega_{io}^{safe}\|\hat{\boldsymbol{p}}_i - \hat{\boldsymbol{p}}_o\| \tag{14}$$

$$P_{io}(\boldsymbol{x}) = \begin{cases} g_{io}^P(\boldsymbol{x}), & if\ g_{io}^P(\boldsymbol{x}) \geq 0 \\ 0, & (otherwise) \end{cases} \tag{15}$$

where $\Omega_{io}^{safe} = R_o^T diag(1/(r_i + a_o + d_{io}^a)^2, 1/(r_i + b_o + d_{io}^b)^2, 1/(r_i + c_o + d_{io}^c)^2)R_o$. Hence, the penalty function is shown as follows.

$$P(\boldsymbol{x}) = P_{ij}(\boldsymbol{x}) + P_{io}(\boldsymbol{x}) \tag{16}$$

3.6 C/GMRES method

In MPC, it is necessary to solve the optimal control problem up to a finite time future to obtain the control input. When controlling robots and UAVs, optimization must be performed in the order of milliseconds, and it is difficult to perform optimization in the control period in

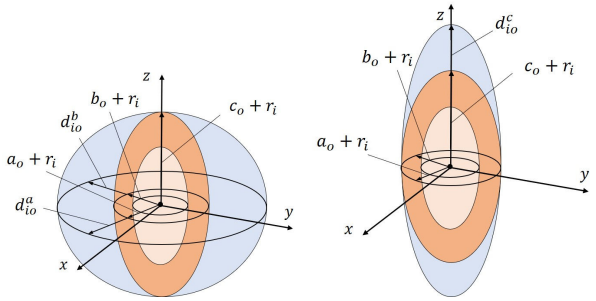

(a) Horizontal Potential Field (b) Vertical Potential Field

Fig. 3.: Setting the Potential Field

iterative optimization methods such as Newton's method. Therefore, we use C/GMRES method, which is a combination of GMRES method and a method without iterative optimization method, as the numerical algorithm. In this numerical algorithm, the optimal control problem is first discretized to derive the nonlinear algebraic equations for the discretized control input sequence. Then, the optimal control sequence as an implicit function of the current state and time is derived. In the update of the control input sequence, under certain conditions, the derivatives of the control input sequence with respect to time is shown by differential equations denoted by the derivative of the state with respect to time. GMRES method can be used to find a solution with sufficient accuracy in a few iterations, because that differential equations involves a large linear equations. In addition, there is no need to compute the Jacobi matrix directly, which reduces the computational cost.

4. NUMERICAL SIMULATION

4.1 Simulation conditions

In this paper, an IBIS with a radius of 0.1 m was used as the control target. Simulation experiments were performed in the MATLAB$^{\mathrm{TM}}$ environment. For the position and velocity data, Gaussian noise with a mean of 0 and a covariance of 0.09^2 m was added as measurement noise. Collision probability thresholds are set to $\delta_r = \delta_o = 0.003$, and the control period was set to $T_s = 0.01$s. The tick width of the prediction time used in CCMPC is $\Delta t = 0.01$s and the number of steps in the prediction is $N = 100$. The predicted horizon, which is the final prediction time, is $T = 1.0$ s.

4.2 Dynamic obstacle avoidance

In this section, we compare the simulation results with MPC using deterministic constraints. The following constraints are used as barrier functions.

$$g_{\ d} = d^2_{safe} - (\boldsymbol{p}_i - \boldsymbol{p}_h)^2 \qquad (17)$$
$$\forall\, h \neq i \in \mathcal{I} \cup \mathcal{I}_o$$

where d_{safe} denotes no-entry area, and we set 0.3 m. In this simulation, three UAVs form a formation, and the UAV moves to the target position following the movement of the formation. The formation coordinates move from (3.0, 3.0 ,0) m to (-3.0, -3.0, 0) m, and the relative positions of the three UAVs in the formation coordinates are always controlled to be $\boldsymbol{p}^1_1 = (0, 0, 0)$ m, $\boldsymbol{p}^1_2 = (1.2, 0.3, 0)$ m, and $\boldsymbol{p}^1_3 = (0.3, 1.2, 0)$ m. The obstacles were a sphere with a radius of 0.4 m and the ellipsoid with axes of (0.2, 0.8, 0.4) m. The initial positions were set to (1.0, -5.0, 0) m and (-3.0, -4.0, 0) m. The velocities were (0, 0.5, 0) m/s, (0.1, 0.3, 0) m/s, and the ellipsoid was tilted by $(\pi/4, 0, \pi/4)$.

The simulation results for CCMPC are shown in Fig.4, and the results for deterministic MPC are shown in Fig.5. The red sphere represents UAV 1, the green and the purple represent UAV 2 and UAV 3 respectively. the blue objects represent the obstacles. Fig. 5 (a) confirms that the trajectory of the UAVs is oscillating. Because of the use of area-based deterministic constraints, the cause of the problem is thought to be that the UAVs in the formation interfere with each other's no-entry area due to sensor errors. In Fig.4 (c), the ellipsoid with the longitudinal direction as the front is approaching, but the UAVs generates the avoidance trajectory in the target direction without difficulties. On the other hand, in Fig.5, the UAV avoids in the direction opposite to the target value, indicating that the avoidance trajectory is not generated in the direction of the target value. In this simulation, we calculated the convergence time, the trajectory length, and the Root Mean Square (RMS) between the position of the UAV and the target value at each time. Table.1 shows the average of the results of five simulation runs. We defined convergence time as the time when the UAV entered the range of 0.2 m from the target and stayed there for more than 3 s. The orbital length and RMS were recorded from the beginning of the simulation until 30 s. For CCMPC and deterministic MPC, there is no difference in convergence time for UAV 1, but the convergence time for UAV 2 and UAV 3 is shorter by 11.9 % and 22.7 % for CCMPC. For UAV 3, the convergence time is the shortest due to the introduction of the collision probability constraint. This may be due to the fact that in deterministic MPC, no-entry area interfered near the target due to sensor error, causing the UAV to temporarily move more than 0.2 m away from the target. On average, the orbital length and RMS of all UAVs are about 13 % shorter for CCMPC. In terms of the orbital length, UAV 3 is the shortest, with an orbital length of approximately -16.0 %. This may be due to the fact that the avoidance trajectory of the ellipsoid was in the opposite direction of the target value. In the RMS, UAV 2 is the shortest at -17.9 %. This may be due to the fact that for both the sphere and ellipsoid obstacles, the UAV avoided in the opposite direction of the target value. In this simulation, UAV 2 and UAV 3 have to pass through a crowded area surrounded by obstacles, so the deterministic constraint is not considered to be able to generate an optimal avoidance trajectory. In addition, since the flight trajectory oscillated due to the mutual interference of the exclusion zones, CCMPC was

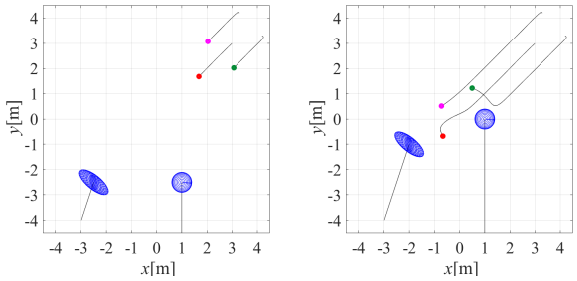

(a) $t = 5\,\mathrm{s}$ (b) $t = 10\,\mathrm{s}$

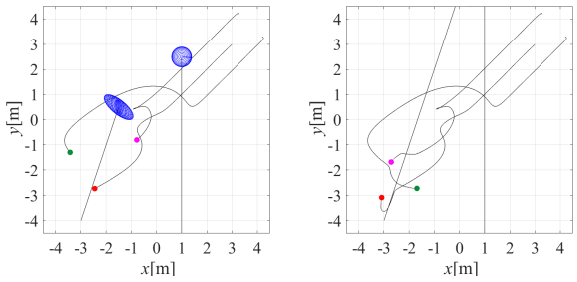

(c) $t = 15\,\mathrm{s}$ (d) $t = 30\,\mathrm{s}$

Fig. 4.: Collision avoidance in dynamic environments using CCMPC (red:UAV 1, green:UAV 2, purple:UAV 3, blue:moving obstacles).

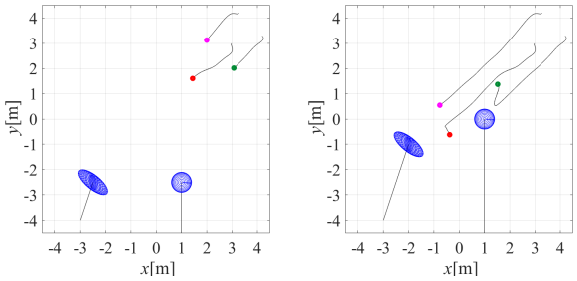

(a) $t = 5\,\mathrm{s}$ (b) $t = 10\,\mathrm{s}$

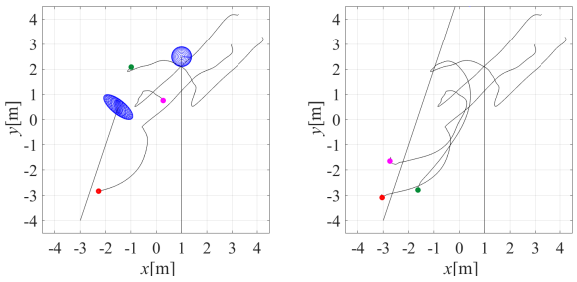

(c) $t = 15\,\mathrm{s}$ (d) $t = 30\,\mathrm{s}$

Fig. 5.: Collision avoidance in dynamic environments using deterministic MPC (red:UAV 1, green:UAV 2, purple:UAV 3, blue:moving obstacles).

considered to be more suitable for operation in formation flight. The UAVs did not avoid the vertical direction.

4.3 Changing formation in formation flight

We simulate a more complex formation change in order to verify the effectiveness of formation flying with CCMPC. The initial formation is a symmetrical V-shape, and the target formation is a pentagon. Each UAV changes formation while moving in the positive direction of the x axis at a speed of 0.3 m/s in accordance with the movement of the formation coordinates. The results of the numerical simulation using CCMPC are shown in Fig.6 and the results of deterministic MPC are shown in Fig.7. Table.2 shows the color, initial position, and target position of each UAV. The z-coordinate is omitted because no vertical movement of the UAVs was observed. After the start of control, each UAV starts to move toward the target position, but in CCMPC, the UAVs moved in parallel in formation as shown in Fig.6 (b) in order to avoid collision. After 10 s, the entire formation rotated around the purple UAV 3 and converged into a pentagonal shape. During the series of formation changes with the movement of the formation, there is no oscillation in the trajectory of the UAV, indicating that it follows a smooth path. On the other hand, with the deterministic constraint, the formation was transformed into a pentagonal formation at about 15 s, as shown in Fig.7 (c). However, the trajectories of all the UAVs showed oscillations during the formation change, especially the purple UAV 2, which showed fine oscillations starting at 10 s. In addition, it can be observed that even after the pentagon deformation, especially for the blue UAV4 and orange UAV5, they do not converge to the target y-coordinate position of -1.0 m. The base of the pentagon is considered to be due to the interference of the mutual constraint conditions because of the close distance between the UAVs.

5. CONCLUSION

In this paper, the effectiveness of CCMPC in formation flight was verified by comparing it with deterministic MPC. In order to reduce the computational cost, we used C/GMRES method for the numerical calculations, and improved the potential field to be designed more flexibly. Since the optimization method with low computational cost is used, it is considered feasible to implement the method in actual UAV. However, since the constraint used in this study only considers the position, it may be difficult to avoid obstacles with acceleration or high velocity. Hence, by introducing speed-aware constraints into CCMPC, it is expected to provide more robust avoidance to changes in the speed of obstacles.

REFERENCES

[1] D. Pines and F. Bohorquez, “Challenges Facing Future Micro-Air-Vehicle Development ”, *AIAA J. Aircraft*, vol.43, no.2, pp.290-305, 2006.

[2] Y. Aida, S. Suzuki, Y. Fujisawa, K. Iizuka, T. Kawamura and Y. Ikeda “Collision-Free Guidance Control for Multiple Small Helicopters” *ICRA*, vol.4, no.4, pp.5537-5543, 2014.

[3] D. H. Shim, H. J. Kim and S. Sastry,“Decentralized Nonlinear Model Predictive Control of Multiple

Table 1.: Comparison of mean values of convergence time, root mean square and orbital length of each UAV in dynamic obstacles avoidance simulation.

	CCMPC			Deterministic MPC		
UAV(i)	Convergence time [s]	Orbital length [m]	RMS [m]	Convergence time [s]	Orbital length [m]	RMS [m]
1	20.2	9.62	1.54	20.4	11.2	1.67
2	22.4	11.9	2.16	25.4	13.2	2.63
3	20.5	10.2	1.82	26.5	12.1	2.06

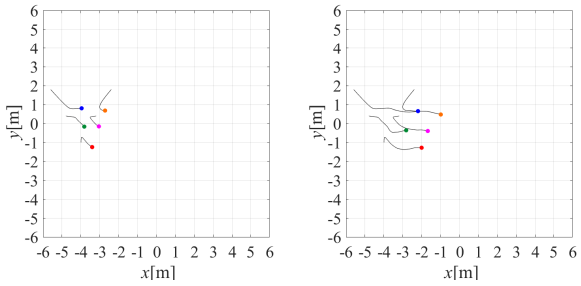

(a) $t = 5\,\mathrm{s}$ (b) $t = 10\,\mathrm{s}$

(c) $t = 15\,\mathrm{s}$ (d) $t = 30\,\mathrm{s}$

Fig. 6.: Formation flight transformation from V-shaped to pentagon using CCMPC.

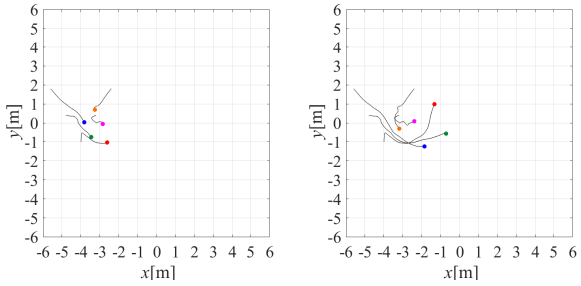

(a) $t = 5\,\mathrm{s}$ (b) $t = 10\,\mathrm{s}$

(c) $t = 15\,\mathrm{s}$ (d) $t = 30\,\mathrm{s}$

Fig. 7.: Formation flight transformation from V-shaped to pentagon using deterministic MPC.

Table 2.: Initial position and target position in formation coordinates, and color of each UAV.

UAV(i)	Color	Initial Position [m]	Target Position [m]
1	Red	(0, -1.0)	(0, 1.0)
2	Green	(-0.8, 0.4)	(1.2, 0.1)
3	Purple	(0.8, 0.4)	(-1.2, 0.1)
4	Blue	(-1.6, 1.8)	(0.7, -1.0)
5	Orange	(1.6, 1.8)	(-0.7, -1.0)

Flying Robots ", in *the 42nd CDC*, pp.3621-3626, 2003.

[4] O. Khatib , "Real-time obstacle avoidance for manipulators and mobile robots", *ICRA*, pp.500-505, 1985.

[5] J. Berg, M. Lin and D. Manocha, "Reciprocal Velocity Obstacles for real-time multi-agent navigation", *ICRA*, pp.1928-1935, 2008.

[6] J.Shin and H.J.Kim, "Nonlinear Model Predictive Formation Flight", in *TSMC - Part A: Systems and Humans*, vol. 39, no.5, pp1116-1125, 2009.

[7] H. Qian, X. Xia and L. Liu, "A Centralized Approach to Flight Conflict Resolution In Multi-Agent System", *2009 First International Workshop on Education Technology and Computer Science*, pp.1063-1065, 2009.

[8] L. E. Kavralu, P. Svestka, J. -. Latombe, and M. H. Overmars, "Probabilistic Roadmaps for Path Planning in High-Dimensional Configuration Spaces", in *Trans. on RA*, vol.12, no.4, pp.566-580, 1996.

[9] J.J. Kuffner and S.M. LaValle, "RRT-Connect : An Efficient Approach to Single-Query Path Planning", in *Proc. IEEE Int. Conf. Robot. Autom.*, San Francisco, CA, pp.995-1001, vol.2, 2000.

[10] H. Zhu and J. Alonso-Mora, "Chance-Constrained Collision Avoidance for MAVs in Dynamic Environments", in *RA-L*, vol.4, no.2, pp.776-783, 2019.

[11] M. Kamel, J. Alonso-Mora, R. Siegwart and J. Nieto, "Robust collision avoidance for multiple micro aerial vehicles using nonlinear model predictive control", *IROS*, pp. 236-243, 2017.

[12] T. Nägeli, L. Meier, A. Domahidi, J. Alonso-Mora and O.Hilliges, "Real- time planning for automated multi-view drone cinematography", *ACM Trans. Graph*, vol. 36, no. 4, Art. no. 132, 2017.

[13] T. Ohtsuka, " A continuation/GMRES Method for Fast Computation of Nonlinear Receding Horizon Control, " in *Automatica*, vol.40, no.4, pp. 563-574, 2004.